WILEY-VCH

High-Performance Colorful Semitransparent Organic Photovoltaics with Microcavity Resonance Color Filter

Xin Liu, Ziping Zhong, Yibin Li, Zhong'an Li, Jie Zhou, Rihong Zhu, Jiangsheng Yu, Gang Li**

X. Liu, Z. Zhong, R. Zhu, J. Yu
School of Electronic and Optical Engineering, Nanjing University of Science and Technology, Nanjing, 210094, China
E-mail: yjs@njust.edu.cn

J. Yu, G. Li
Department of Electronic and Information Engineering, The Hong Kong Polytechnic University, Hong Kong, China
E-mail: gang.w.li@polyu.edu.hk

Y. Li, Z. Li
School of Chemistry and Chemical Engineering, Huazhong University of Science and Technology, Wuhan, 430074, China

J. Zhou
School of Chemistry and Chemical Engineering, Nanjing University of Science and Technology, Nanjing 210094, China

Keywords: semitransparent organic photovoltaics, microcavity resonance color filter, color tunability, transmitted/reflected color, photostability

Abstract:

Microcavity resonance is an effective technique for making promising semitransparent organic photovoltaics (ST-OPVs) even more aesthetically attractive with high color saturation, by tailoring the visible transmittance spectrum to narrow transmission peak. In this study, a distinctive microcavity resonance color filter (CF) structure of silver/ bismuth(III) fluoride /silver (Ag/BiF_3/Ag) is integrated upon the rear transparent electrode, which simultaneously achieves high color purity and high power conversion efficiency (PCE) for colorful ST-OPVs. By precisely regulating the thickness of BiF_3 layer, we achieve ST-OPVs with a wide color gamut with high color purity, including the colors of indigo, blue, bluish-green, green, orange, and red, as well as compound color devices with dual or multiple transmission peaks in visible region. A recorded PCE of 16.27% is obtained for the indigo ST-OPVs, with the CIE 1931

coordinates of (0.164, 0.087) and a maximum transmittance of 18.7% at the transmission peak wavelength of 393 nm. Furthermore, we systematically investigate CF-based ST-OPVs as color reflectors under different light incident surfaces. The improved stability of CF-based devices is attributed to the excellent moisture resistance of BiF_3. The colorful ST-OPVs with desired transmitted/reflected colors, and wide color gamut show great potential for future energy harvesting solutions.

1. Introduction

Organic photovoltaics (OPVs) have attracted significant interest for their exceptional benefits such as solution processability, flexibility, light weight, and optical semitransparency, which make them suitable for various potential applications.[1-6] Recently, the power conversion efficiency (PCE) of single junction and tandem OPVs has exceeded 19%,[7-9] and the light utilization efficiency (LUE) for semitransparent OPVs (ST-OPVs) has also reached 5.35% through comprehensive optimizations, including ternary strategy, materials screening, and band-pass transparent electrode.[10]

ST-OPVs have shown great potential in building surfaces, power windows, mobile terminals, wearable devices, agricultural applications, and other areas. Visual color transparency and photoelectric functionalities are critical for these important applications.[11-16] The device color of ST-OPVs is mainly dictated by the absorption spectra of active layer and electrode.[17-18] Previous efforts to develop colorful ST-OPVs focused on the assembly of donor and acceptor materials with tailored optical bandgaps. However, owing to the broad absorption spectra of organic active layer materials, it is challenging to develop colorful devices by fine-tuning the combination of bulk-heterojunction. Furthermore, a thin metal layer, such as silver (Ag) or gold (Au), is commonly used as the rear electrode of ST-OPVs, which limits the transmittance or reflectance spectrum, resulting in non-selective color.

Incorporating light manipulation optical structure is a distinct toute and an effective approach for manufacturing colorful ST-OPVs. Numerous optical structures, such as chromatic plasmonic polarizers (CPP)[19-23], optical spacers[24], one-dimensional photonic-crystals (1DPCs)[25-27], induced transmission filters (ITFs)[28-31], and microcavity resonance color filter (CF)[32-39] have been investigated in OPVs for chromatic devices. For instance, Fatemeh et al[23] designed a CPP electrode in OPVs by employing a hybrid nanostructure of graphene and aluminum nano-cross arrays as electrode, in which the transmission color is tuned by controlling the polarization of the incident light or transmission light. Meriem et al[24] described the fabrication of Al-doped zinc oxide (AZO) nanocrystals that can modulate the color by altering the thicknesses of optical spacers and active layer blends. Shen et al[27] tuned the position and intensity of the optical Tamm state into ST-OPVs via integrating the electrode of Ag, an extra additional layer, and 1DPCs. Wang et al[31] proposed spectrally selective electrodes by combining ITF, conductive metal film, anti-reflective coating, and hydrophobic surface, resulting in narrow optical bandpass ST-OPVs with high PCE and long-term stability. Compared to the above optical structures, integrating an optical CF into ST-OPV is a very effective method to obtain various colored devices. Typically, the architecture of CF is metal layer/optical resonance layer/metal layer, meaning that only two extra layers are required upon routine ST-OPVs. The resonance mode is determined by the optical resonance condition of the microcavity[40-41]: $L(\lambda) = \sum n_i d_i + \frac{\lambda}{4\pi}(\psi_1 + \psi_2) = m\frac{\lambda}{2}$, where λ is the wavelength of the incident light; n_i and d_i denote the refractive index and thickness of the layers within the microcavity, respectively; ψ_1 and ψ_2 are the reflection shift of the cavity mirrors; and m is a positive integer. 2L(λ)/ λ is calculated to obtain the resonance mode of the microcavity. In CF-based devices, strong microcavity resonance can be achieved, which exploits the resonance mode to selectively transmit specific wavelengths of light while reflecting the rest into the active layer. Metal oxidize materials, such as titanium dioxide (TiO_2), silicon dioxide (SiO_2),

tungsten trioxide (WO_3), Indium tin oxide (ITO), molybdenum oxide (MoO_3), tellurium oxide (TeO_2), and antimony oxide (Sb_2O_3), are widely chosen as the optical resonance layer. During the sputtering or electron beam evaporation processes for the widely used TiO_2, SiO_2, WO_3, or ITO, the involved high temperatures can damage active layer in device, leading to inferior photovoltaic performance. Therefore, it is crucial to explore the optical resonance layer that utilizes optical materials with suitable refractive indices and lossless parasitic absorption via "non-destructive" thermal evaporation or solution processes. Additionally, reflected color and stability are also essential for the commercial application of colorful ST-OPVs, which have rarely been addressed in the literature.

In this study, bismuth(III) fluoride (BiF_3) is firstly utilized as the optical resonance layer to fabricate CF-based colorful ST-OPVs due to its process flexibility through thermal evaporation, a low melting point of about 719 °C[42], low coefficient of thermal expansion, a high refractive index of 1.81 at a corresponding wavelength of 550 nm, and excellent transmittance in the visible and NIR regions with a forbidden bandwidth of approximately 3.94 eV. An inverted device architecture of glass/ ITO/ zinc oxide (ZnO)/ active layer/ molybdenum trioxide (MoO_3)/ Ag (inner)/ BiF_3/ Ag (rear) is investigated for colorful ST-OPVs. Considering the high transmission peak and narrow full width at half maximum (FWHM) of devices, the Ag thickness on the inner and rear sides is chosen at 30 nm to achieve high color purity. The transmittance spectra of CF-based ST-OPVs are calculated using the transfer matrix method (TMM) to regulate the thickness of BiF_3 layer. The CF-based ST-OPVs have a single transmission peak in the visible region when the microcavity resonance mode is first-order. Dual or multiple transmission peaks can be controlled by the increase of resonance modes. The high-performing active layers, PM6: BTP-eC9 have been used to investigate the potential of CF-based colorful ST-OPVs. By varying the thickness of the BiF_3 layer (44, 67, 83, 101, 115, and 130 nm), ST-OPVs with a wide range of vivid colors were successfully fabricated,

including indigo, blue, bluish-green, green, orange, and red. A remarkable PCE of 16.27% was obtained for the indigo ST-OPVs, with a maximum transmittance (T_{max}) of 18.7% at a peak wavelength of 393 nm and the Commission Internationale de l´Eclairage (CIE) 1931 coordinates of (0.164,0.087). Other colorful ST-OPVs also exhibited high PCEs approaching 16%, which are retained over 90% compared to that of the opaque device (16.94%). Exploring the universality of CF structures, three active layer systems with different optical bandgaps, PTB7-Th: $PC_{71}BM$ (1.57eV), PM6: Y6 (1.33eV), and PTB7-Th: IEICO-4F (1.29eV), were utilized to fabricate RGB (red, green, and blue) ST-OPVs. Transmitted/ reflected color properties of the corresponding devices were systematically investigated. For individual CF structure, the reflected color is complementary to the transmitted color. For CF based ST-OPVs, the reflected color is consistent with the color of the CF structure when light is incident on the back surface (Ag surface). Whereas, when light is incident on the front surface (glass surface), the reflected colors of colorful ST-OPVs are affected by the absorption of active layer due to multilayer film interference effect. Furthermore, the BiF_3 layer has strong moisture resistance and can be employed as a buffer layer for device encapsulation. Compared with ST-OPV without CF, the CF-based ST-OPV exhibited improved long-term and light soaking stability. Our results indicate the simplicity and effectiveness of BiF_3-based CF structures for constructing high-performing, colorful ST-OPVs, which have significant potential for building-integrated photovoltaics (BIPVs) integration and diversified approaches to the future of energy harvesting.

2. Results and Discussion

2.1. Design and Fabrication of CF Electrodes

A distinctive microcavity resonance CF structure of Ag (inner)/ BiF_3/ Ag (rear) was investigated in this study to obtain color properties by tuning the thickness of BiF_3 layer. The

transmission peak and FWHM of the CF structure are strongly correlated with the thickness of the Ag layer. Considering the inner Ag layer as part of the CF structure and also as the electrode of the ST-OPVs device, the electrode needs a thickness of over 10 nm to ensure conductive properties.[14] The TMM method[43-45] was used to simulate the transmittance curves of CF structures of glass/ Ag (10, 20, 30, and 40 nm)/ BiF_3/ Ag (30 nm), as shown in Figure S1 and Figure S2, Supporting Information. The thickness of BiF_3 was set to 80 nm for simplified calculations. Comparing these CF structures, the symmetrical Ag-Ag microcavity exhibited a higher intensity resonance effect with a high transmission peak of 46.9% at 494 nm and a narrow FWHM of 51.9 nm when 30 nm Ag was selected as the inner electrode in Table S1, Supporting Information. Meanwhile, the transmittance spectrum distribution of glass/ Ag (0-50 nm)/ BiF_3 (80 nm)/ Ag (0-50 nm) CF structures are simulated in the case of symmetrical Ag-Ag thickness in **Figure 1**a. We further gathered the simulated data of the glass/ Ag (10, 20, 30, 40, and 50 nm)/ BiF_3 (80 nm)/ Ag (10, 20, 30, 40, and 50 nm) CF structures in Figure S3 and Table S2. As the thickness of the inner and rear Ag increases, the transmittance spectrum distribution exhibits a narrower FWHM, along with a lower transmission peak. Considering the trade-off between transmission peaks and FWHM, the 30-nm Ag thicknesses of the inner and the rear were preferential.

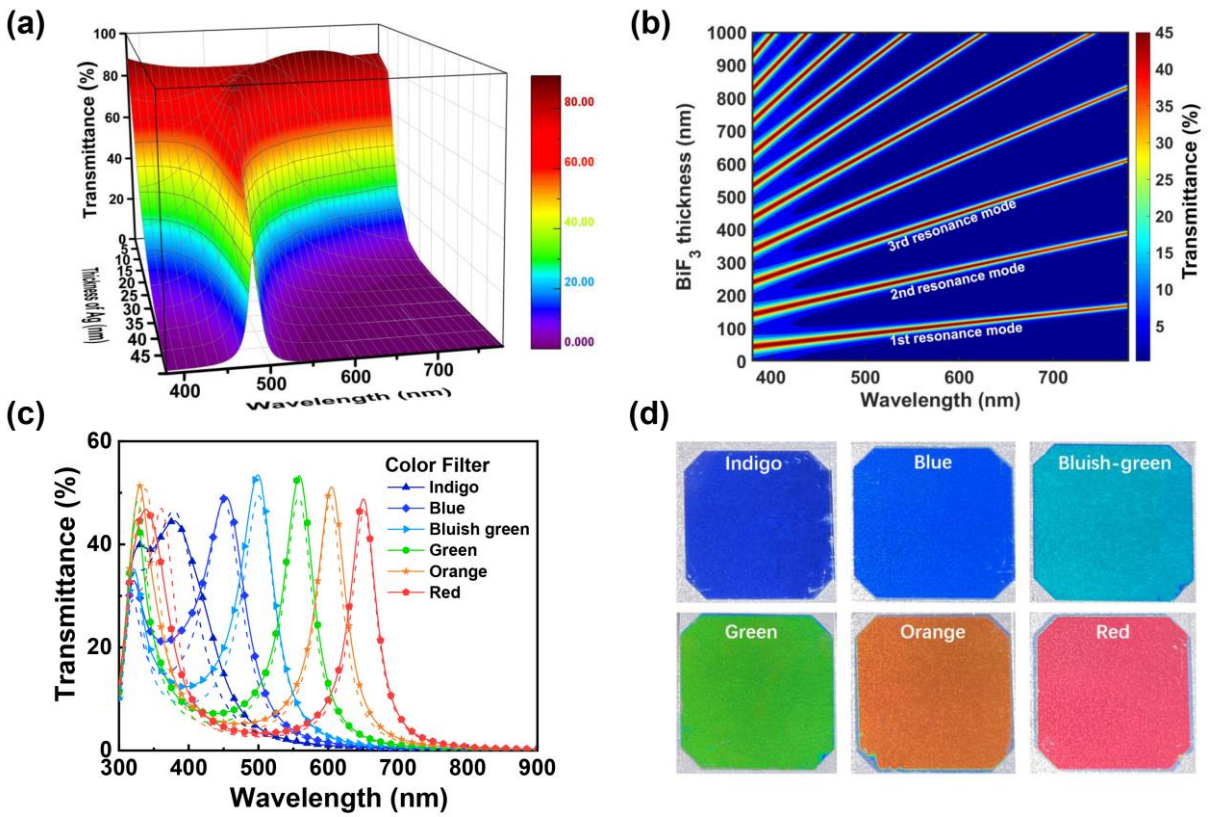

Figure 1. The simulated transmittance spectra of (a) glass/ Ag (0~50 nm)/ BiF_3 (80 nm)/ Ag (0~50 nm) and (b) glass/ Ag (30 nm)/ BiF_3(0~1000 nm)/ Ag (30 nm) CF structures. (c) The simulated (dashed lines) and experimental (solid lines) transmittance spectra of glass/ Ag (30 nm)/ BiF_3 (44, 67, 83, 101, 115, and 130 nm)/ Ag (30 nm) CF structures. (d) Digital images of indigo, blue, bluish-green, green, orange, and red CFs using one sunlight (solar simulator) illuminated through a white paper on the CFs.

The relationship between the BiF_3 thickness of the microcavity resonance and the transmittance spectrum distribution was further explored to optimize the CFs with symmetrical 30-nm Ag layers as shown in **Figure 1**b. The resonance modes[36] are obtained when the BiF_3 thickness is varied from 0 to 1000 nm. By tuning the BiF_3 thickness, the transmission peak can span the broad visibile region from 380 to 780 nm. In the first-order resonance mode (BiF_3 thickness ranging from 0 to 150 nm), the red-shift peak appears as the thickness of BiF_3 increases. In the second-order resonance mode (BiF_3 thickness ranging from 150 to 230 nm), the CF exhibits a higher color purity and narrower FWHM of transmittance spectrum than that in the first-order resonance mode. For instance, when the transmission peak wavelength is set at 448 nm, the thickness of BiF_3 should be set at 65 or 185 nm for first- or second-order,

respectively, as shown in Figure S4a, Supporting Information. The FWHM values of the first-, and second-order transmittance spectrum are 65.37 and 30.25 nm, respectively (Table S3, Supporting Information). The second-order resonance mode can achieve higher blue purity for ST-OPVs, but the transmission peak is limited to the 380-520 nm range (Figure S4b, Supporting Information). It is worth noting that mixed colors resulting from dual transmission peaks in visibile region can be obtained due to the synergistic effect of second-order and third-order resonance modes, when the BiF_3 thickness is varied from 230 nm to 320 nm. For instance, the BiF_3 optical layer thicknesses were selected at 250, 270, and 290 nm to simulate the transmittance spectrum. Consequently, dual transmittance peaks of relative CFs appear in the visibile region as shown in Figure S4c and Table S3, Supporting Information, and the corresponding color coordinates were depicted in Figure S4d, Supporting Information. As the resonance mode increases, more transmission peaks and various colorful devices can be obtained.

Based on the above analysis, colorful CFs within the first-order resonance mode are fabricated using vacuum deposition techniques. Six colors, namely indigo, blue, bluish-green, green, orange, and red were selected for manipulation of CFs with the structure of glass/ Ag (30 nm)/ BiF_3 (0~150 nm)/ Ag (30 nm). The BiF_3 thicknesses based on simulation were defined at 44, 67, 83, 101, 115, and 130 nm, respectively. As shown in **Figure 1**c**,** the simulated and experimental transmittance spectra of the corresponding CFs are matched well. The detailed optical parameters were summarized in Table S4 and Table S5, Supporting Information, respectively. The experimental indigo, blue, bluish-green, green, orange, and red CFs exhibit center of resonance transmission peaks at 393, 446, 492, 551, 594, and 649 nm, respectively, and almost equal intensity of transmission peaks at about 50%. Among them, the green CF has the highest average visible transmittance (AVT) of 27.11% due to the overlap of the transmittance spectrum distribution with the photopic curve of human eye.[46] **Figure 1**d shows

the digital photographs of the fabricated CFs (1.5 ×1.5 cm^2) illuminated from glass surface using white paper as the background. The distinct colorful CFs exhibit different color coordinates (x, y) of (0.1794, 0.1145), (0.1599, 0.1142), (0.1586, 0.3256), (0.3428, 0.5099), (0.4996, 0.3901), and (0.4985, 0.3165) for indigo, blue, bluish-green, green, orange, and red devices, respectively. The CIE 1931 chromaticity values of corresponding CFs were depicted in Figure S5, Supporting Information. In general, in the first-order resonance mode, it is simple to obtain CFs with high color purity by varying the thickness of BiF_3.

2.2. Application of CF electrodes for ST-OPVs

To highlight the potential of CF in ST-OPVs, devices were fabricated with the inverted configuration of glass/ ITO/ ZnO/ active layers/ MoO_3/ Ag (30 nm)/ BiF_3 (0~150 nm)/ Ag (30 nm) as illustrated in **Figure 2**a. The high-performing PM6: BTP-eC9[47-49] system was utilized as organic active layer (Figure S6 and Figure S7, Supporting Information). For comparison, opaque devices and normal ST-OPVs were fabricated with solely 150-nm and 30-nm Ag layers, respectively. CF-based devices were fabricated with BiF_3 layers of thickness at 44, 67, 83, 101, 115, and 130 nm for indigo, blue, bluish-green, green, orange, and red ST-OPVs, respectively.

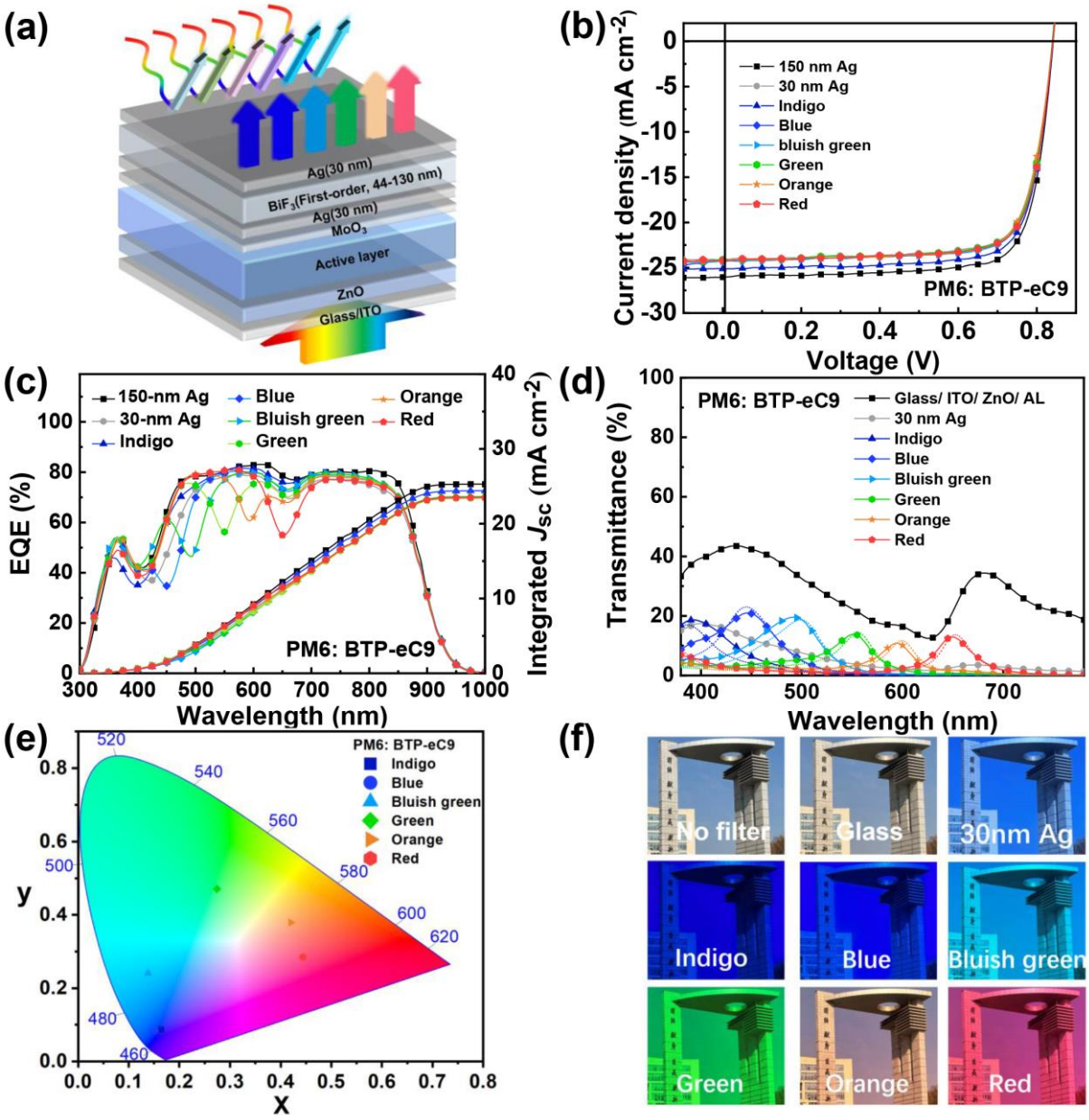

Figure 2. (a) Schematic representation of CF-based ST-OPVs with the inverted configuration of glass/ ITO/ ZnO (30 nm)/ active layer /MoO_3 (8 nm)/ Ag (30 nm)/ BiF_3 (0-150 nm)/ Ag (30 nm). (b) Current-voltage (*J*-*V*) curves and (c) external quantum efficiency (EQE) curves of 150-nm Ag OPVs, 30-nm Ag ST-OPVs, and colorful CF-based ST-OPVs. (d) Simulated (dash lines) and experimental (solid lines plus symbol) transmittance spectra. (e) The CIE 1931 chromaticity of CF-based ST-OPVs according to the experimental transmittance spectra, and (f) digital camera images of indigo, blue, bluish-green, green, orange, and red CF-based ST-OPVs with Nanjing University of Science and Technology (NJUST) landmark building as background.

The current-voltage (*J*-*V*) curves and corresponding photovoltaic parameters are summarized in **Figure 2**b and **Table 1**. The opaque device exhibited a PCE of 16.94% with a short circuit current density (J_{SC}) of 26.04 mA cm^{-2}, an open-circuit voltage (V_{OC}) of 0.841 V, and a fill

factor (FF) of 77.34%.[50] 30-nm Ag ST-OPV exhibited a considerable PCE of 15.52% with a J_{SC} of 24.07 mA cm^{-2}, V_{OC} of 0.839 V, and FF of 76.86%. The slightly lower J_{SC} of 30-nm Ag ST-OPV can be attributed to the semitransparent of 30-nm Ag (AVT of 4.03%), resulting in a relatively lower PCE. CF-based ST-OPVs yielded PCEs of 16.27%, 15.75%, 15.78%, 15.60%, 15.63%, and 15.70% for indigo, blue, bluish-green, green, orange, and red devices, respectively. To the best of our knowledge, the PCE of 16.27% is the highest PCE value for colorful ST-OPVs in the literature (Table S6, Supporting Information).

The CF-based ST-OPVs exhibited similar V_{OC} and FF, while the various PCEs were attributed to the J_{SC} distribution. Compared to the *J*sc of opaque device, CF-based ST-OPVs exhibited photocurrent losses of 3.70%, 7.38%, 7.16%, 7.92%, 7.47%, and 7.60% for indigo, blue, bluish-green, green, orange and red ST-OPVs, respectively, which is consistent with the decreasing trend in PCE. Notably, the green ST-OPV demonstrated a higher AVT and PCE compared to the bare 30-nm Ag-based one. This result suggests that ST-OPVs can incorporate the green CF structures to improve the LUE values. To verify these trends, the EQE curves (**Figure 2**c**)** and transmittance spectra (**Figure 2**d) of corresponding devices were measured. The trough-shaped EQE curves are corresponded to the same wavelength center as the peak transmittance of each device. EQE(λ), Transmittance(T(λ)), and Reflectance (R(λ)) were measured to minimize experimental errors, and carry out photon balancing checks for each ST-OPV[51]. All T(λ) + R(λ) + EQE(λ) values of CF-based ST-OPVs are below 1, indicating the reliability and accuracy of the results (Figure S8, Supporting Information). The T_{max} of large area (1.5 × 1.5 cm^2, Figure S9, Supporting Information) indigo, blue, bluish-green, green, orange, and red ST-OPVs, were 18.70% at 393 nm, 21.00% at 446 nm, 19.60% at 492 nm, 13.80% at 551 nm, 10.80% at 594 nm, and 12.90% at 649 nm, respectively (**Table 1**). The integrated J_{SC} values from EQE curves are 24.41, 23.55, 23.63, 23.44, 23.53, and 23.51 mA

cm^{-2} for indigo, blue, bluish-green, green, orange, and red ST-OPVs, respectively. The results are in accordance with the values obtained from *J-V* measurements. As shown in **Figure 2**e and **Table 1**, various CF-based ST-OPVs with different CIE 1931 coordinates were achieved, namely indigo (0.164, 0.087), blue (0.152, 0.085), bluish-green (0.138, 0.241), green (0.274, 0.471), orange (0.420, 0.379), and red (0.444, 0.285). And CF-based ST-OPVs exhibited high transparency and vivid color saturation for the landmark building of NJUST (**Figure 2**f), highlighting its potential for BIPVs integration applications (Figure S10, Supporting Information).

Table 1. Photovoltaic performances and optical parameters of 150-nm Ag OPV, 30-nm Ag, and CF-based ST-OPVs using PM6: BTP-eC9 as active layer.

Device	J_{SC} (mA/cm^2) [a]	J_{SC}^{EQE} (mA/cm^2) [b]	V_{OC} (V) [a]	FF (%) [a]	PCE (%) [a]	Center of resonance (nm)	Peak transmittance (%)	CIE 1931 (x, y)	AVT (%)
150-nm Ag	26.04 (25.73 ± 0.27)	25.29	0.841 (0.840 ± 0.01)	77.34 (77.01 ± 0.31)	16.94 (16.64 ± 0.25)	-	-	-	-
30-nm Ag	24.07 (23.81 ± 0.24)	23.39	0.839 (0.838 ± 0.01)	76.86 (76.45 ± 0.35)	15.52 (15.25 ± 0.27)	-	-	(0.212, 0.214)	4.03
Indigo	25.11 (24.73 ± 0.21)	24.41	0.839 (0.838 ± 0.01)	77.24 (77.02 ± 0.20)	16.27 (15.98 ± 0.23)	393	18.7	(0.164, 0.087)	0.71
Blue	24.25 (23.92 ± 0.29)	23.55	0.840 (0.838 ± 0.02)	77.32 (76.86 ± 0.44)	15.75 (15.41 ± 0.31)	446	21.0	(0.152, 0.085)	1.65
Bluish-green	24.30 (23.95 ± 0.32)	23.63	0.840 (0.838 ± 0.02)	77.29 (76.83 ± 0.39)	15.78 (15.42 ± 0.32)	492	19.6	(0.138, 0.241)	4.23
Green	24.13 (23.80 ± 0.31)	23.44	0.839 (0.838 ± 0.01)	77.05 (76.70 ± 0.30)	15.60 (15.30 ± 0.28)	551	13.8	(0.274, 0.471)	6.85
Orange	24.23 (23.89 ± 0.28)	23.53	0.840 (0.838 ± 0.02)	76.77 (76.54 ± 0.21)	15.63 (15.32 ± 0.26)	594	10.8	(0.420, 0.379)	4.62
Red	24.20 (23.85 ± 0.29)	23.51	0.840 (0.838 ± 0.02)	77.24 (76.88 ± 0.31)	15.70 (15.37 ± 0.30)	649	12.9	(0.444, 0.285)	2.04

[a] The statistical values are obtained from the 12 devices. [b] The integrated current densities from EQE curves.

2.3. Theoretical Simulation

The transmittance spectrum distribution of the CF-based ST-OPVs as a function of BiF_3 optical layer thickness and visible wavelength range distribution is depicted in **Figure 3**a, which exhibits similar optical properties to those of the bare CF structures. The simulated transmittance spectra of the devices are highly consistent with the experimental ones, indicating the simplicity and effectiveness of BiF_3-based CF structures for constructing targeted colorful ST-OPVs. Compared to 150-nm Ag based OPV, 30-nm Ag based devices exhibited a lower intensity optical electric field distribution due to photon transmittance loss. For CF-based ST-OPVs, the intensity distribution of the optical electric field in active layer shows a significant reduction in the transmission area which is corresponding to its transmittance spectrum. And an enhanced intensity distribution of the optical electric field within the CF occurs due to optical interference. These simulations indicate that the optical electric field distributions are highly dependent on wavelength and inhomogeneous due to optical interference effects.

Figure S11 (Supporting Information) shows the simulated exciton generation rate[52-54] of PM6: BTP-eC9 based devices to explore the trend of J_{SC} values. The resonance light can be selectively transmitted by the CF structure while non-resonance light is reflected. Obviously, the exciton generation rate in the 150-nm Ag based OPV is maximum. Comparing 30-nm Ag ST-OPV to colored one, the distribution of exciton generation rate was changed due to the optical interference effect throughout the whole active layer. For instance, compared to 30-nm Ag based device, green ST-OPV exhibited a significantly decreased exciton generation rate in the transmission area (500-600 nm). While the exciton generation rates were enhanced in the non-transmission area. The simulated J_{SC} values are in consistence with the experimental results.

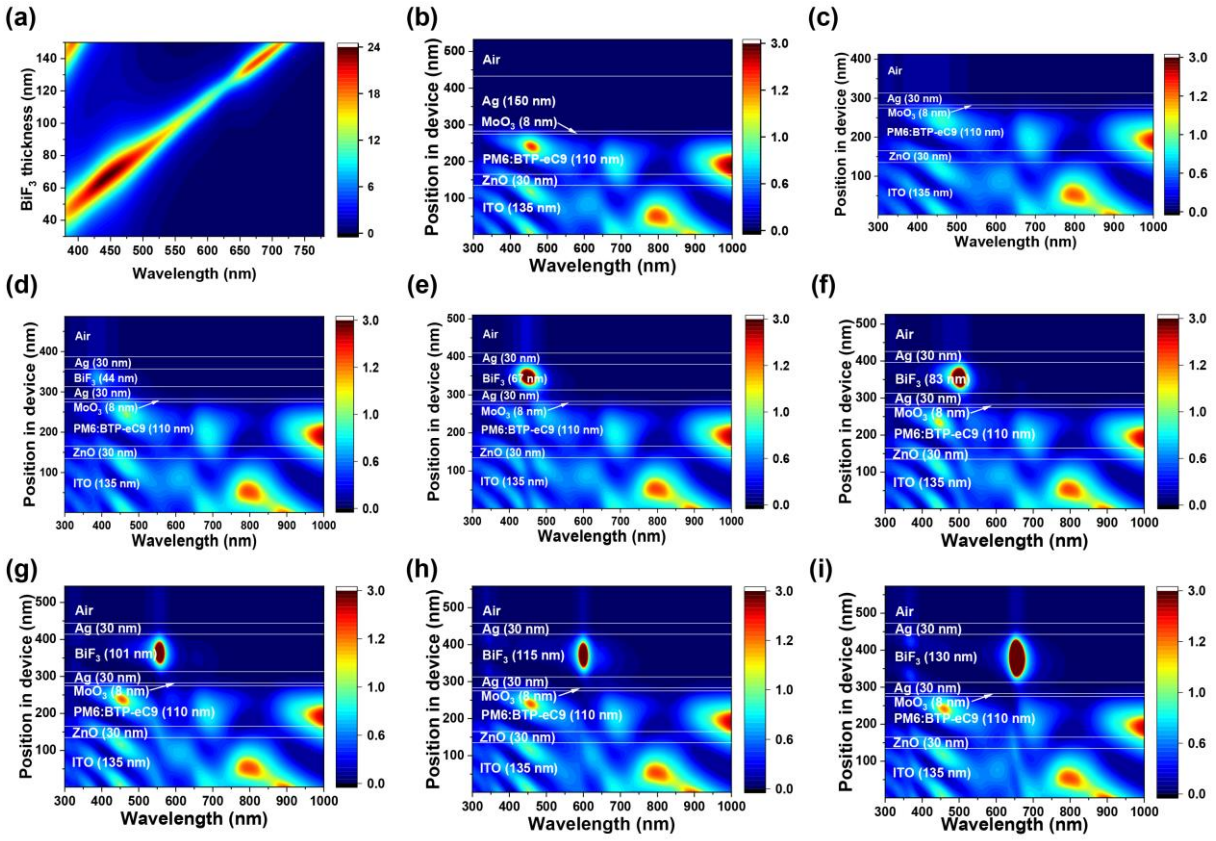

Figure 3. (a) The simulated transmittance spectrum of the CF-based ST-OPVs as a function of wavelength and BiF_3 thickness. The simulated electric field intensity profile $|E|^2$ of the (b) 150-nm Ag OPV, (c) 30-nm Ag, (d) indigo, (e) blue, (f) bluish-green, (g) green, (h) orange and (i) red ST-OPVs, the active layer material of these devices using PM6: BTP-eC9 system.

2.4. CF-based ST-OPVs as Color Reflectors

The reflected colors of CF-based ST-OPVs were explored when light is incident on different surfaces. The reflectance spectra of CF structures were recorded with front and back surfaces as shown in Figure S12, Supporting Information. The reflectance spectra of Ag/ BiF_3/ Ag-based CF show the same resonance peaks, indicating that the reflected colors of CF structures remain the same when the light is incident on different surfaces. The reflected colors of CF-based ST-OPVs were further analyzed as shown in **Figure 4**. The front (**Figure 4**a) and back (**Figure 4**c) reflectance spectra of the same CF-based ST-OPV were distinctly different. When light is incident on the front surface, it produces a blue reflected color due to the strong absorption of PM6: BTP-eC9 in the 500-800 nm (**Figure 4**b). Nevertheless, when light is incident on back surface, the reflected color of CF-based ST-OPV is consistent with the color of corresponding

CF, owing to the strong microcavity resonance of the CF (**Figure 4**d). In general, the multilayer thin film interference effect leads to diverse reflected colors on the front surface of the colorful devices, while the consistency of the reflected colors on the back surface under the same CF structure is attributed to the strong microcavity resonance effect.

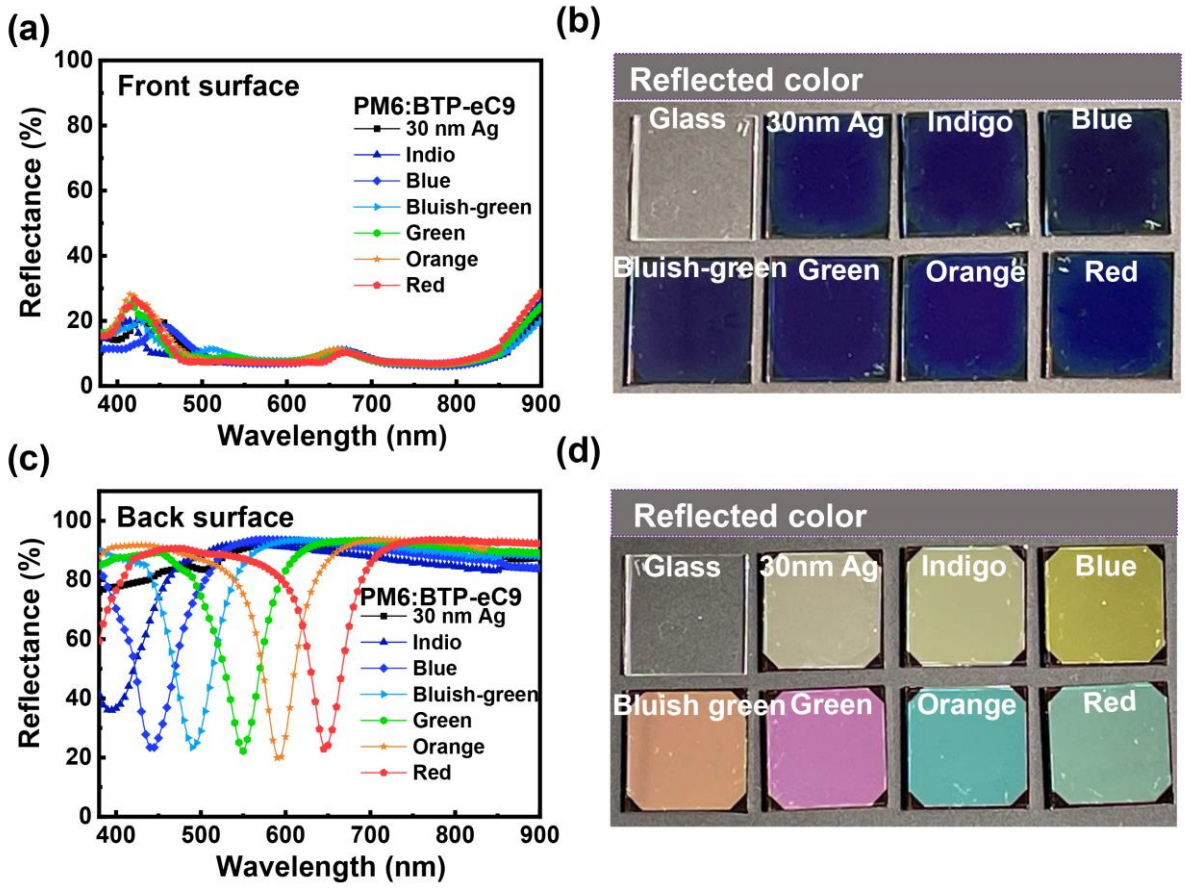

Figure 4 The CF-based ST-OPVs have a structure of glass/ ITO/ ZnO/ PM6:BTP-eC9/ MoO_3/ Ag (30 nm)/ BiF_3 (44, 67, 83, 101, 115, and 130 nm)/ Ag (30 nm). (a) Measured reflectance spectra when sunlight is incident on the front surface. (b) The images of reflected colors when sunlight is incident on the front surface upon an opaque black plate. (c) Measured reflectance spectra when sunlight is incident on the back surface. (d) The images of reflected colors when sunlight is incident on the back surface upon an opaque black plate.

2.5. Universality of CF electrodes for ST-OPVs

To demonstrate the universality of BiF_3-based CF for colorful ST-OPVs, we have fabricated RGB devices using various active layers with different bandgaps (Figure S7, Supporting Information), including PTB7-Th: $PC_{71}BM$ (1.57eV), PM6: Y6 (1.33eV), and PTB7-Th: IEICO-4F (1.29eV). Figure S13, Supporting Information, shows the corresponding *J*-*V* and

EQE curves, and the transmittance spectra of the devices in the visible region. For the PM6: Y6 based RGB devices, the blue one exhibits an excellent device performance with a PCE of 14.27% with a high T_{max} of 23.8% at 445 nm peak wavelength. Due to the uniformly weak absorption of PTB7-Th:$PC_{71}BM$ layer in the visible region, all the PTB7-Th:$PC_{71}BM$ based colorful ST-OPVs reveal high T_{max} over 20%. The green one exhibit the highest peak transmittance of 27.0% at 558 nm. PTB7-Th: IEICO-4F-based blue or green devices exhibit the highest T_{max} of 34.9% at 443 nm, and 29.9% at 552 nm, respectively. The results show that the peak wavelength is determined by the CF structure, while the intensity of T_{max} is closely related to the absorption of the active layer. The detailed photovoltaic and optical characteristics, T(λ) + R(λ) + EQE(λ) values, the CIE 1931 coordinates, optical simulation, and images were also summarized in Table S7 and Figure S14-23, Supporting Information, respectively.

The reflected colors of CF-based ST-OPVs using three different active layers were studied with emphasis. The front and back reflectance spectra of the CF-based ST-OPVs were measured and presented in Figure S24 and Figure S25, Supporting Information. In terms of front surface, the different absorption distribution of the three active layer systems (PTB7-Th: $PC_{71}BM$, PM6: Y6, and PTB7-Th: IEICO-4F) resulted in different reflected colors, as shown in Figure S24d, Supporting Information. The visible absorption of PTB7-Th: $PC_{71}BM$ and PTB7-Th: IEICO-4F is weak, and the frontal reflected color of their devices is affected by both the active layer material and the CF structure due to the multilayer film interference effect. The absorption of PM6: Y6 is similar to that of PM6: BTP-eC9. Strong absorption of PM6: Y6 between 500 and 800 nm results in a blue reflected color of device when light is incident on the front surface. When light is incident on the back surface (Figure S25d, Supporting Information), the reflected color of the CF-based ST-OPVs (PTB7-Th: $PC_{71}BM$, PM6: Y6, and PTB7-Th: IEICO-4F) is consistent with the color of the CF structure due to the strong microcavity resonance effect, indicating the effective color management of Ag/ BiF_3/ Ag-based CF structures.

2.6. Long-term Stability Measurements

In addition to the excellent optical manipulation properties, CF structures are also highly stable due to strong moisture resistance of BiF_3 film, which are utilized as a buffer layer for the encapsulation of ST-OPVs. In order to visualize the effect of BiF_3 optical layer on moisture and oxygen, the equivalent encapsulation test was explored[10]. Calcium metal is very sensitive to oxygen and moisture, and is widely used in the OLED industry for packaging and stability testing. We fabricated devices with two structures, Glass/Ca (200 nm) and Glass/Ca (200 nm)/BiF_3 (150 nm), using calcium metal as the test layer. The devices were stored in air, and the change of transmittance was measured (Figure S26, Supporting Information). After storage in air (Temperature of 26 °C and Humidity of 60%) for less than 8 min, the transmittance of Glass/ Ca (200 nm) devices without BiF_3 optical layer is almost equal to the transmittance of Glass, indicating that Ca is rapidly oxidized. In contrast, the transmittance curves of Glass/ Ca (200 nm)/BiF_3 (150 nm) devices after 30 h of air storage are almost unchanged, indicating that the barrier performance of the integrated device with BiF_3 optical layer is significantly improved. The equivalent packaging testing results imply that employing the BiF_3 optical layer can effectively prolong the stability of inner layer (Ca) in air. To test the stability of the devices, we followed the ISOS-D-1 and ISOS-L-1 protocols.[55-56] For ISOS-D-1, the encapsulated devices were placed in a dark room with a temperature of 25°C in a glove box. For ISOS-L-1, the encapsulated device is placed in a glove box at 25°C under LED light conditions. The intensity of LED light was calibrated by a standard silicon cell and operated under one sun (**Figure 5**)**,** where the digital lux meter shows a value of 274600 lux. The corresponding spectrum of LED light is located at 420-700 nm (Figure S27, Supporting Information).

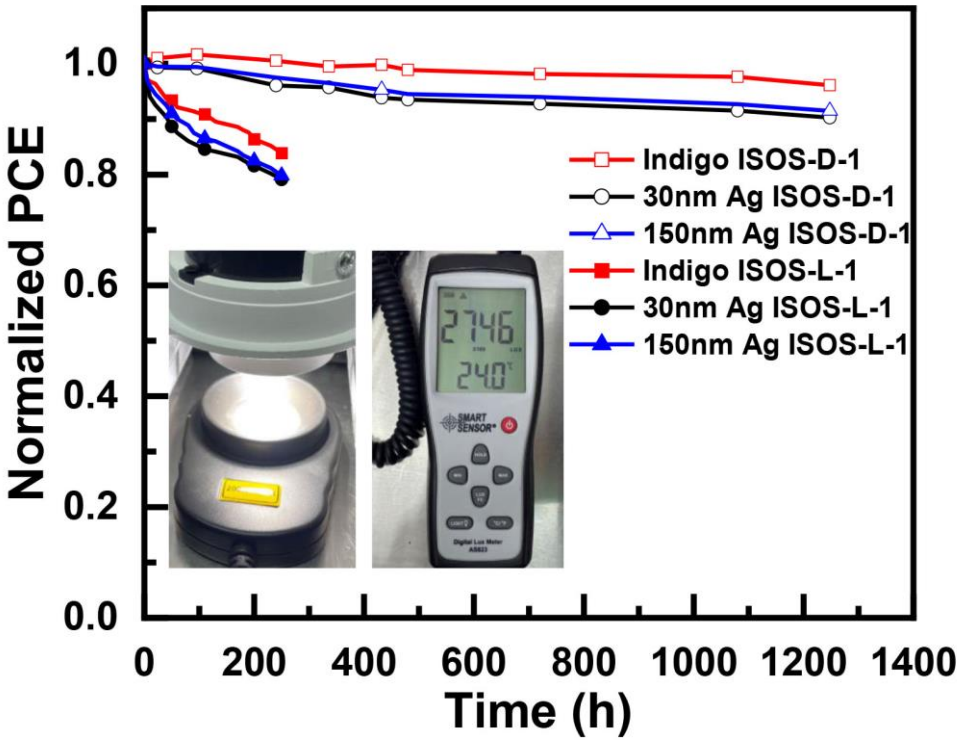

Figure 5 Normalized PCE of indigo ST-OPV in comparison to 30-nm and 150-nm Ag based OPVs as a function of time upon dark and light conditions. The inset is a picture of the device stability test system.

A systematic comparison was analyzed between encapsulated indigo, 30-nm and 150-nm Ag OPVs under conditions based on the ISOS-D-1 and ISOS-L-1 protocols (Figure S28, Supporting Information). After 1200-h storage under the ISOS-D-1 protocol, the PCEs of indigo, 30-nm and 150-nm Ag based ST-OPVs remained 96%, 90% and 91% of the initial PCE, respectively. Under the ISOS-L-1 protocol, the device performance is significantly degraded. After 250 h of light soaking, the PCE of the indigo ST-OPV device maintained 83% of its initial PCE, while the PCE of the 30-nm and 150-nm Ag OPVs device showed over 20% of PCE loss (**Figure 5)**. The enhanced device stability of colored devices can be attributed to the role of the Ag/ BiF_3/ Ag optical layer as a buffer layer in the encapsulation.

3. Conclusion

In conclusion, a versatile resonance CF structure with the BiF_3 as optical layer is successfully integrated into ST-OPVs to manipulate the color. By controlling the thickness of BiF_3 layer,

the microcavity resonance transmission peak in the visible region can be regulated. As a result, the CF structure of 30-nm Ag/ BiF_3 (44, 67, 83, 101, 115, and 130-nm)/ 30-nm Ag was utilized for fabricating ST-OPVs with indigo, blue, bluish-green, green, orange and red colors. CF-based ST-OPVs show superior optical performance with narrow FWHM as low as 40 nm and high transmission peak of 10.8-34.9%, resulting in vivid color saturation. The PM6:BTP-eC9 colorful ST-OPVs exhibited a high PCE of over 15.6%, which can maintain over 92% of the PCE of opaque device. An outstanding efficiency of 16.27% was achieved for indigo ST-OPVs with a transmission peak approaching 20% at 393 nm, which is the highest value for colorful ST-OPVs ever reported. The transmitted and reflected colors of individual CF structures are complementary. When the light is incident on the front surface, the reflected colors of CF-based ST-OPVs are affected by both the absorption of active layer and the CF structure due to the multilayer film interference effect. While the reflected colors are mainly determined by the strong microcavity resonance when the light is incident on the back surface. The improved device stability of CF based ST-OPVs also indicated Ag/BiF_3/Ag structures can be employed as a buffer layer in the encapsulation. In summary, the Ag/BiF_3/Ag based CFs reveal effective color tuning capability, offering a new avenue for high-performing colorful ST-OPVs.

Supporting Information

Supporting Information is available from the Wiley Online Library or from the author.

Acknowledgements

The authors gratefully acknowledge the financial support of the National Natural Science Foundation of China (No. 21905137) and Jiangsu Planned Projects for Postdoctoral Research Funds (No. 2021K554C). J. Yu thanks the support from the Hong Kong Scholar Program (XJ2020042) and the Fundamental Research Funds for the Central Universities. G. Li thanks the support from Research Grants Council of Hong Kong (GRF 152221320, CRF C5037-18G,

SRFS2223-5S01), Hong Kong Polytechnic University (Sir Sze-yuen Chung Endowed Professorship Fund (8-8480), G-SAC5)

Conflict of Interest

The authors declare no conflict of interest.

Data Availability Statement

The data that support the findings of this study are available from the corresponding author upon reasonable request.

Received: ((will be filled in by the editorial staff))
Revised: ((will be filled in by the editorial staff))
Published online: ((will be filled in by the editorial staff))

Reference

[1] G. Yu, J. Gao, J. C. Hummelen, F. Wudl, A. J. Heeger, *Science* **1995**, 270, 1789.

[2] G. Li, V. Shrotriya, J. Huang, Y. Yao, T. Moriarty, K. Emery, Y. Yang, *Nature Materials* **2005**, 4, 864.

[3] J. Y. Kim, K. Lee, N. E. Coates, D. Moses, T. Q. Nguyen, M. Dante, A. J. Heeger, *Science* **2007**, 317, 222.

[4] R. Søndergaard, M. Hösel, D. Angmo, T. T. Larsen-Olsen, F. C. Krebs, *Materials Today* **2012**, 15, 36.

[5] S.-H. Bae, H. Zhao, Y.-T. Hsieh, L. Zuo, N. De Marco, You S. Rim, G. Li, Y. Yang, *Chem* **2016**, 1, 197.

[6] G. Li, C.-W. Chu, V. Shrotriya, J. Huang, Y. Yang, *Appl. Phys. Lett.* **2006**, 88, 253503.

[7] Y. Cui, Y. Xu, H. Yao, P. Bi, L. Hong, J. Zhang, Y. Zu, T. Zhang, J. Qin, J. Ren, Z. Chen, C. He, X. Hao, Z. Wei, J. Hou, *Adv. Mater.* **2021**, 33, 2102420.

[8] J. Wang, Z. Zheng, Y. Zu, Y. Wang, X. Liu, S. Zhang, M. Zhang, J. Hou, *Adv. Mater.* **2021**, 33, 2102787.

[9] Z. Zheng, J. Wang, P. Bi, J. Ren, Y. Wang, Y. Yang, X. Liu, S. Zhang, J. Hou, *Joule* **2022**, 6, 171.

[10] X. Liu, Z. Zhong, R. Zhu, J. Yu, G. Li, *Joule* **2022**, 6, 1918.

[11] E. Ravishankar, R. E. Booth, C. Saravitz, H. Sederoff, H. W. Ade, B. T. O'Connor, *Joule* **2020**, 4, 490.

[12] W. Song, B. Fanady, R. Peng, L. Hong, L. Wu, W. Zhang, T. Yan, T. Wu, S. Chen, Z. Ge, *Adv. Energy Mater.* **2020**, 10, 2000136.

[13] Q. Fan, R. Ma, Z. Bi, X. Liao, B. Wu, S. Zhang, W. Su, J. Fang, C. Zhao, C. Yan, K. Chen, Y. Li, C. Gao, G. Li, W. Ma, *Adv. Funct. Mater.* **2023**, 33, 2211385.

[14] X. Liu, Y. Zhao, J. Yu, R. Zhu, *Mater. Chem. Front.* **2021**, 5, 8197.

[15] D. Wang, H. Liu, Y. Li, G. Zhou, L. Zhan, H. Zhu, X. Lu, H. Chen, C.-Z. Li, *Joule* **2021**, 5, 945.

[16] D. Wang, Y. Li, G. Zhou, E. Gu, R. Xia, B. Yan, J. Yao, H. Zhu, X. Lu, H.-L. Yip, H. Chen, C.-Z. Li, *Energy Environ. Sci.* **2022**, 15, 2629.

[17] Y. Wong, H.-F. Meng, H. Wong, C. Tan, C.-Y. Wu, P.-T. Tsai, C.-Y. Chang, S.-F. Horng, H.-W. Zan, *Org. Electron.* **2017**, 43, 196.

[18] D. Yang, T. Sano, H. Sasabe, L. Yang, S. Ohisa, Y. Chen, Y. Huang, J. Kido, *ACS Appl. Mater. Interface* **2018**, 10, 26465.

[19] T. Ellenbogen, K. Seo, K. B. Crozier, *Nano Lett.* **2012**, 12, 1026.

[20] S. Sun, Z. Ye, L. Guo, N. Sun, *J. Opt. Soc. Am. B* **2014**, 31, 1211.

[21] M. A. Mahmoud, *J. Phys. Chem. C* **2016**, 120, 18249.

[22] K. Saito, T. Tatsuma, *Nanoscale* **2017**, 9, 18624.

[23] F. F. Mahani, A. Mokhtari, *Opt. Mater.* **2018**, 84, 158.

[24] M. Gaceur, S. B. Dkhil, D. Duché, F. Bencheikh, J.-J. Simon, L. Escoubas, M. Mansour, A. Guerrero, G. Garcia-Belmonte, X. Liu, M. Fahlman, W. Dachraoui, A. K. Diallo, C. Videlot-Ackermann, O. Margeat, J. Ackermann, *Adv. Funct. Mater.* **2016**, 26, 243.

[25] W. J. Dong, N.-T. Lo, G. H. Jung, J. Ham, J.-L. Lee, *Appl. Phys. Lett.* **2016**, 108, 103902.

[26] Y. Zhang, Z. Peng, C. Cai, Z. Liu, Y. Lin, W. Zheng, J. Yang, L. Hou, Y. Cao, *J. Mater. Chem. A* **2016**, 4, 11821.

[27] P. Shen, M. Yao, J. Liu, Y. Long, W. Guo, L. Shen, *J. Mater. Chem. A* **2019**, 7, 4102.

[28] R. J. Holloway, P. H. Lissberger, *Appl. Opt.* **1969**, 8, 653.

[29] D. T. Owens, C. Fuentes-Hernandez, J. M. Hales, J. W. Perry, B. Kippelen, *Opt. Express* **2010**, 18, 19101.

[30] A. Sytchkova, *Appl. Opt.* **2011**, 50, C90.

[31] S. Wang, J. Chen, L. Li, L. Zuo, T.-Y. Qu, H. Ren, Y. Li, A. K.-Y. Jen, J.-X. Tang, *ACS Nano* **2020**, 14, 5998.

[32] Y.-H. Chen, C.-W. Chen, Z.-Y. Huang, W.-C. Lin, L.-Y. Lin, F. Lin, K.-T. Wong, H.-W. Lin, *Adv Mater* **2014**, 26, 1129.

[33] Y. Kim, J. Son, S. Shafian, K. Kim, J. K. Hyun, *Adv. Opt. Mater.* **2018**, 6, 1800051.

[34] J.-H. Lu, Y.-H. Lin, B.-H. Jiang, C.-H. Yeh, J.-C. Kao, C.-P. Chen, *Adv. Funct. Mater.* **2018**, 28, 1703398.

[35] S. Shafian, J. Son, Y. Kim, J. K. Hyun, K. Kim, *ACS Appl. Mater. Interfaces* **2019**, 11, 18887.

[36] J. Zhong, Z. Xiao, W. Liang, Y. Wu, Q. Ye, H. Xu, H. Deng, L. Shen, X. Feng, Y. Long, *ACS Appl. Mater. Interfaces* **2019**, 11, 47992.

[37] X. Li, R. Xia, K. Yan, J. Ren, H.-L. Yip, C.-Z. Li, H. Chen, *ACS Energy Lett.* **2020**, 5, 3115.

[38] H. R. Yeom, S. Song, S. Y. Park, H. S. Ryu, J. W. Kim, J. Heo, H. W. Cho, B. Walker, S.-J. Ko, H. Y. Woo, J. Y. Kim, *Nano Energy* **2020**, 77, 105146.

[39] Y.-M. Sung, M.-Z. Li, D. Luo, Y.-D. Li, S. Biring, Y.-C. Huang, C.-K. Wang, S.-W. Liu, K.-T. Wong, *Nano Energy* **2021**, 80, 105565.

[40] M. Agrawal, P. Peumans, *Opt. Express* **2008**, 16, 5385.

[41] Y. Long, *Appl. Phys. Lett.* **2009**, 95, 193301.

[42] T. J. Moravec, R. A. Skogman, E. Bernal G, *Appl. Opt.* **1979**, 18, 105.

[43] L. A. A. Pettersson, L. S. Roman, O. Inganäs, *J. Appl. Phys.* **1999**, 86, 487.

[44] P. Peumans, A. Yakimov, S. R. Forrest, *J. Appl. Phys.* **2003**, 93, 3693.

[45] G. F. Burkhard, E. T. Hoke, M. D. McGehee, *Adv Mater* **2010**, 22, 3293.

[46] Y. Bai, F. Han, R. Shi, F. Wang, S. Jiang, J. Wang, Z. Tan, *Sol. RRL* **2022**, 6, 2200174.

[47] Y. Cai, Y. Li, R. Wang, H. Wu, Z. Chen, J. Zhang, Z. Ma, X. Hao, Y. Zhao, C. Zhang, F. Huang, Y. Sun, *Adv. Mater.* **2021**, 33, 2101733.

[48] X. Chen, D. Wang, Z. Wang, Y. Li, H. Zhu, X. Lu, W. Chen, H. Qiu, Q. Zhang, *Chem. Eng. J.* **2021**, 424, 130397.

[49] W. Peng, Y. Lin, S. Jeong, Z. Genene, A. Magomedov, H. Woo, C. Chen, W. Wahyudi, Q. Tao, J. Deng, Y. Han, V. Getautis, W. Zhu, T. D. Anthopoulos, E. Wang, *Nano Energy* **2022**, 92, 106681.

[50] H. Gao, X. Wei, R. Yu, F.-Y. Cao, Y. Gong, Z. Ma, Y.-J. Cheng, C.-S. Hsu, Z. Tan, *Adv. Opt. Mater.* **2022**, 10, 2102031.

[51] C. Yang, D. Liu, M. Bates, M. C. Barr, R. R. Lunt, *Joule* **2019**, 3, 1803.

[52] E. Gondek, *Opt. Mater.* **2013**, 36, 98.

[53] F. Wang, B. Zhang, Q. Li, Z. Shi, L. Yu, H. Liu, Y. Wang, S. Dai, Z. Tan, Y. Li, *J. Mater. Chem. A* **2016**, 4, 1915.

[54] Y. Bai, C. Zhao, X. Chen, S. Zhang, S. Zhang, T. Hayat, A. Alsaedi, Z. Tan, J. Hou, Y. Li, *J. Mater. Chem. A* **2019**, 7, 15887.

[55] M. O. Reese, S. A. Gevorgyan, M. Jørgensen, E. Bundgaard, S. R. Kurtz, D. S. Ginley, D. C. Olson, M. T. Lloyd, P. Morvillo, E. A. Katz, A. Elschner, O. Haillant, T. R. Currier, V. Shrotriya, M. Hermenau, M. Riede, K. R. Kirov, G. Trimmel, T. Rath, O. Inganäs, F. Zhang, M. Andersson, K. Tvingstedt, M. Lira-Cantu, D. Laird, C. McGuiness, S. Gowrisanker, M. Pannone, M. Xiao, J. Hauch, R. Steim, D. M. DeLongchamp, R. Rösch, H. Hoppe, N. Espinosa, A. Urbina, G. Yaman-Uzunoglu, J.-B. Bonekamp, A. J. J. M. van Breemen, C. Girotto, E. Voroshazi, F. C. Krebs, *Solar Energy Materials and Solar Cells* **2011**, 95, 1253.

[56] M. V. Khenkin, E. A. Katz, A. Abate, G. Bardizza, J. J. Berry, C. Brabec, F. Brunetti, V. Bulović, Q. Burlingame, A. Di Carlo, R. Cheacharoen, Y.-B. Cheng, A. Colsmann, S. Cros, K. Domanski, M. Dusza, C. J. Fell, S. R. Forrest, Y. Galagan, D. Di Girolamo, M. Grätzel, A. Hagfeldt, E. von Hauff, H. Hoppe, J. Kettle, H. Köbler, M. S. Leite, S. Liu, Y.-L. Loo, J. M. Luther, C.-Q. Ma, M. Madsen, M. Manceau, M. Matheron, M. McGehee, R. Meitzner, M. K. Nazeeruddin, A. F. Nogueira, Ç. Odabaşı, A. Osherov, N.-G. Park, M. O. Reese, F. De Rossi, M. Saliba, U. S. Schubert, H. J. Snaith, S. D. Stranks, W. Tress, P. A. Troshin, V. Turkovic, S. Veenstra, I. Visoly-Fisher, A. Walsh, T. Watson, H. Xie, R. Yıldırım, S. M. Zakeeruddin, K. Zhu, M. Lira-Cantu, *Nat. Energy* **2020**, 5, 35.

Ag/BiF_3/Ag based color filter (CF) reveal effective color tuning capability. The indigo CF-based ST-OPV achieves a recorded power conversion efficiency of 16.27% with a maximum transmittance of 18.7% at a peak wavelength of 393 nm. Versatile colorful ST-OPVs with wide color gamut, reflected color characteristics and improved stability offer a new avenue for building-integrated photovoltaic applications.

Xin Liu, Ziping Zhong, Yibin Li, Zhong'an Li, Jie Zhou, Rihong Zhu, Jiangsheng Yu[*], *Gang Li*[*]

High-Performance Colorful Semitransparent Organic Photovoltaics with Microcavity Resonance Color Filter

ToC figure